The Meteoritical Society

Meteoritics & Planetary Science 53, Nr 6, 1267–1282 (2018)
doi: 10.1111/maps.13075

Check for updates

An experimental study on impact-induced alterations of planetary organic simulants

Yasuhito SEKINE[1*], Kenya KODAMA[2], Takamichi KOBAYASHI[3], Seiji OBATA[2], Yu CHANG[1], Nanako O. OGAWA[4], Yoshinori TAKANO[4], Naohiko OHKOUCHI[4], Koichiro SAIKI[2], and Toshimori SEKINE[5]

HPSTAR 562-2018

[1]Department of Earth and Planetary Science, The University of Tokyo, 7-3-1 Hongo, Bunkyo, Tokyo 113-0033, Japan
[2]Department of Complexity Science and Engineering, The University of Tokyo, Kashiwa, Chiba 277-8561, Japan
[3]National Institute for Materials Science, Tsukuba, Ibaraki 305-0044, Japan
[4]Department of Biogeochemistry, JAMSTEC, Yokosuka, Kanagawa 237-0061, Japan
[5]Center for High Pressure Science and Technology Advanced Research, 1690 Cailun Road, Shanghai 201203, China
[*]Corresponding author. E-mail: sekine@eps.s.u-tokyo.ac.jp

(Received 04 August 2017; revision accepted 21 February 2018)

Abstract–The present study systematically investigates shock-induced alteration of organic simulants of planetary bodies (OSPBs) as a function of peak shock pressure and temperature by impact experiments. Our results show that the composition and structure of OSPBs are unchanged upon impacts at peak pressures ≤~5 GPa and temperatures ≤~350 °C. On the other hand, these are dramatically changed upon impacts at >7–8 GPa and > ~400 °C, through loss of hydrogen-related bonds and concurrent carbonization, regardless of the initial compositions of OSPBs. Compared with previous results on static heating of organic matter, we suggest that shock-induced alteration cannot be distinguished from static heating only by Raman and infrared spectroscopy. Our experimental results would provide a proxy indicator for assessing degree of shock-induced alteration of organic matter contained in carbonaceous chondrites. We suggest that a remote-sensing signature of the 3.3–3.6 μm absorption due to hydrogen-related bonds on the surface of small bodies would be a promising indicator for the presence of less-thermally-altered (i.e., <350 °C) organic matter there, which will be a target for landing to collect primordial samples in sample-return spacecraft missions, such as Hayabusa2 and OSIRIS-REx.

INTRODUCTION

Organic matter is commonly found in carbonaceous meteorites and on volatile-rich solid bodies, such as C-type asteroids, dwarf planets, comets, and icy satellites (e.g., Sandford et al. 2006; Cody et al. 2008; Waite et al. 2009; Campins et al. 2010; Postberg et al. 2011; Goesmann et al. 2015; De Sanctis et al. 2017). This organic matter may have been originally formed by chemical reactions in molecular clouds (e.g., Bernstein et al. 1995; Greenberg et al. 1995), heterogeneous reactions in the protoplanetary disk (e.g., Llorca and Casanova 2000; Hill and Nuth 2003; Sekine et al. 2005, 2006), and/or aqueous chemistry within the planetary bodies (e.g., Cody et al. 2011; Kebukawa et al. 2013; Sekine et al. 2017).

Using destructive and nondestructive methods, the chemical structure of insoluble organic matter (IOM) isolated from carbonaceous chondrites has been studied (e.g., Derenne and Robert [2010] and references therein). For instance, the Murchison meteorite contains more aromatic hydrocarbons (including polyaromatic hydrocarbons) than aliphatic hydrocarbons (aromatic C/aliphatic C = ~3) together with nitrogen (mainly as pyrrole N), oxygen (mainly as ether, alcohols, and carboxylic compounds), and sulfur (mainly as aliphatic sulfides) in its structure (Derenne and Robert 2010). IOMs contain high-molecular-weight polyaromatic hydrocarbons (PAH) containing several-ring PAH units that are cross-linked together (Sephton et al. 2004). Aliphatic structures in IOMs would work as bridges between these PAH units (Remusat et al. 2005). The wide variations in stable isotopic compositions of C and N for different chemical structures of chondritic organic matter indicate highly heterogeneous distribution of

these isotopes (e.g., Sephton et al. 2003). Although this organic matter would provide clues for understanding chemical evolution that occurred in the solar system, it may have experienced metamorphism by long-duration static heating due to radionuclides and/or by short-duration heating due to an impact (e.g., Quirico et al. 2003, 2009, 2014; Busemann et al. 2007; Cody et al. 2008; Yabuta et al. 2010). These alteration processes could have changed or overprinted the primordial chemical information.

Recent advances in micro-spectrometry, e.g., Raman and infrared (IR) spectroscopy, for organic matter enable examination of its thermal alteration history (e.g., Yabuta et al. 2005, 2010; Busemann et al. 2007; Cody et al. 2008; Quirico et al. 2014). For instance, the previous studies have proposed that the abundance of C-H bonds and presence of polyaromatic compounds in IOM in carbonaceous chondrites are promising indicators for assessing degree of thermal alteration (Yabuta et al. 2005, 2010; Busemann et al. 2007; Cody et al. 2008; Quirico et al. 2014). These evaluations of thermal alteration of IOMs are based on a comparison with both experimental results of static heating of synthetic organic matter and chemical analyses of natural coal that underwent different degrees of thermal alteration (e.g., Ferrari and Robertson 2001; Quirico et al. 2005). Although these studies are useful to evaluate the maturity of IOMs by long-term static heating, impact-induced shock heating cannot be directly evaluated due to a lack of systematic impact experiments and chemical analyses for recovered organic matter.

Experimental investigations of impact-induced alteration of organic matter are also useful for spacecraft missions targeting collection and in situ chemical analysis of organic matter on volatile-rich bodies (Tsou et al. 2012; McKay et al. 2014; Sekine et al. 2014; Takano et al. 2014). For instance, the Hayabusa2 spacecraft and the Small Carry-on Impactor (SCI) device will perform a high-velocity impact experiment onto C-type asteroid Ryugu (provisional designation, 1999 JU3) to excavate surface materials and will collect subsurface interior samples within the crater (Tachibana et al. 2014; Saiki et al. 2016; Watanabe et al. 2017). Enceladus' plume contains organic matter and silicates, which may have formed under hydrothermal conditions within the core (Hsu et al. 2015; Sekine et al. 2015; Waite et al. 2017). In future missions to Enceladus, collection and in situ analyses of plume materials are proposed during flyby of the plume (e.g., Tsou et al. 2012; McKay et al. 2014). In these missions, captured samples may have experienced some degree of shock during collection or excavation. Shock experiments and chemical analysis for the recovered organic matter also can provide a threshold velocity for intact sampling of organic matter in these spacecraft missions.

In the present study, we performed shock recovery experiments to investigate impact-induced alterations of extraterrestrial organic matter analogs (hereafter, we call these as organic simulants of planetary bodies or OSPBs). The OSPBs were produced by aqueous reactions of organic molecules that are typically contained in comets (Cody et al. 2011; Kebukawa et al. 2013) (also see the Methods section for details). We investigate alterations of the structure and composition of OSPBs caused by hypervelocity impacts using IR and Raman spectroscopy, and elemental and isotope analyses. We then discuss the mechanisms of impact-induced alterations as a function of peak shock pressure and temperature. Finally, we compare our results with the previous data of Raman spectrometry for IOMs collected from carbonaceous chondrites and discuss implications for intact sampling of ongoing and future spacecraft missions.

METHODS

Synthesis of Organic Simulants of Planetary Bodies

We produced OSPBs through the polymerization of formaldehyde (CH_2O), glycolaldehyde ($C_2H_4O_2$), and ammonia (NH_3) using high-temperature aqueous chemistry based on the methodology described in previous studies (Cody et al. 2011; Kebukawa et al. 2013; Sekine et al. 2017). The chemical composition and molar structure of OSPBs are suggested to be similar to those of IOM in carbonaceous chondrites (Cody et al. 2011; Kebukawa et al. 2013). As these aldehydes and ammonia would have been commonly found in comets (e.g., Bockelée-Morvan et al. 2004; Goesmann et al. 2015), these starting materials are also likely to have been contained in building materials of icy bodies in the outer solar system, including Enceladus, Ceres, and Pluto. Given the possible presence of hydrothermal environments within Enceladus (Hsu et al. 2015; Sekine et al. 2015; Waite et al. 2017), Ceres (De Sanctis et al. 2016), and Pluto (Sekine et al. 2017), OSPB-like organic matter may exist in the interiors and surfaces of these bodies.

In the present study, we produced four types of OSPBs for shock recovery experiments by varying the NH_3 contents (NH_3 content = 0.3% and 2% relative to H_2O) in starting solutions, and by varying the formation temperatures (130 and 200 °C). The OSPBs formed from 2% NH_3 solution (hereafter referred to as high-NH_3 OSPBs) may be an analog of organic matter generated within icy bodies whose building materials

Table 1. Impact conditions, and achieved peak shock pressure and temperatures.

OSPB sample	OSPB:quartz mixing ratio	Impact velocity (km s^{-1})	Peak shock pressure (GPa)	Hugenoit temperature (°C)
Low-NH_3 130 °C	1:7	0.639 ± 0.004	2.61 ± 0.02	230
	1:7	0.827 ± 0.005	4.49 ± 0.03	330
	1:7	1.340 ± 0.007	8.53 ± 0.06	550
	1:20	1.614 ± 0.021	11.05 ± 0.20	700
Low-NH_3 200 °C	1:7	0.629 ± 0.006	2.57 ± 0.03	230
	1:7	0.749 ± 0.006	3.17 ± 0.04	300
	1:7	1.150 ± 0.008	6.93 ± 0.06	460
	1:20	1.607 ± 0.015	10.98 ± 0.14	700
High-NH_3 130 °C	1:30	0.598 ± 0.003	2.42 ± 0.01	220
	1:7	0.859 ± 0.006	4.71 ± 0.04	340
	1:7	1.171 ± 0.004	7.10 ± 0.03	470
	1:20	1.659 ± 0.020	11.49 ± 0.19	730
High-NH_3 200 °C	1:30	0.626 ± 0.001	2.55 ± 0.01	230
	1:7	0.816 ± 0.005	3.51 ± 0.03	330
	1:7	1.153 ± 0.007	6.95 ± 0.05	460
	1:20	1.626 ± 0.014	11.16 ± 0.14	710

originated from the outer solar system beyond the NH_3 snowline in the protoplanetary disk (Alibert and Mousis 2007; De Sanctis et al. 2015). A 2% NH_3 content in the starting solution is comparable to reported NH_3 contents in comets and Enceladus' plume (Bockelée-Morvan et al. 2004; Waite et al. 2009). On the other hand, the OSPBs formed from 0.3% NH_3 solution (hereafter referred to as low-NH_3 OSPBs) can be an analog of organic matter formed in icy bodies at relatively inner regions of the protoplanetary disk, e.g., outer regions of the Main Belt. The NH_3 content of 0.3% in the solution is same as that used in Kebukawa et al. (2013), which attempted to produce organic matter similar to primitive chondritic IOM.

We produced a starting solution of 1 mL of pure water containing 60 mg (2 mmol) of CH_2O in the form of paraformaldehyde, 60 mg (1 mmol) of $C_2H_4O_2$, 54 or 540 μL of 10% NH_4OH solution, and 15 mg of calcium hydroxide ($Ca[OH]_2$). Addition of $Ca(OH)_2$ is to ensure a solution with an alkaline pH, as suggested for water in carbonaceous chondrites (Zolotov 2012) and in Enceladus' hydrothermal environments (Glein et al. 2015; Hsu et al. 2015; Sekine et al. 2015). Calcium hydroxide also acts as a catalyst for the formose reaction (Ricardo et al. 2004). The concentrations of CH_2O and $C_2H_4O_2$ in the starting solutions are the same as those of Kebukawa et al. (2013). The solutions were sealed within Pyrex glass tubes and isothermally heated at 130 or 200 °C for 72 h. During heating, OSPBs were produced in the glass tubes. After heating, the mixture of solution and OSPBs were centrifuged at 2500 rpm for 30 min to remove the solution. To remove Ca ions, the precipitated OSPBs were washed with 2 mL of 1 M HCl. The washed OSPBs were centrifuged again to remove the residual solution. This process was repeated twice in all. To remove Cl ions, the precipitated OSPBs were then washed with 40 mL of pure H_2O and centrifuged, a process that was repeated five times. Finally, the precipitated OSPBs were dried in an oven at 70 °C for more than 24 h.

Shock Recovery Experiments

To make the targets for our shock recovery experiments, OSPBs were mixed with quartz (SiO_2) powder using an agate mortar at the mass mixing ratio (OSPBs: quartz) of 1:7, 1:20, and 1:30 (Table 1). The large proportions of quartz were used so that the peak pressure and temperature achieved in the target could be calculated assuming that the target materials are composed of quartz, whose Hugenoit parameters are well known (e.g., Marsh 1980). In addition, we used quartz because it is chemically inert and less likely to affect alteration reactions of the OSPBs. The mixed powder of OSPBs and quartz was introduced into a stainless steel (SUS 304L) container (Fig. 1) and pressed at 24 MPa with a hydraulic press. The diameter and thickness of the sample space in the container are 12 and 3 mm, respectively. The porosity of the resultant samples were measured to be <1%.

Shock recovery experiments were conducted with a propellant gun at the National Institute for Materials Science (NIMS) in Japan (e.g., Sekine 1997; Kobayashi 2014, 2016). A metallic aluminum (Al 6061) or stainless steel (SUS 304) impactor plate (ϕ29 mm in diameter and 2 mm in thickness) was used. The impactor was made to collide onto the stainless steel container at velocities ranging from ~0.60 to 1.66 km s^{-1} (Table 1).

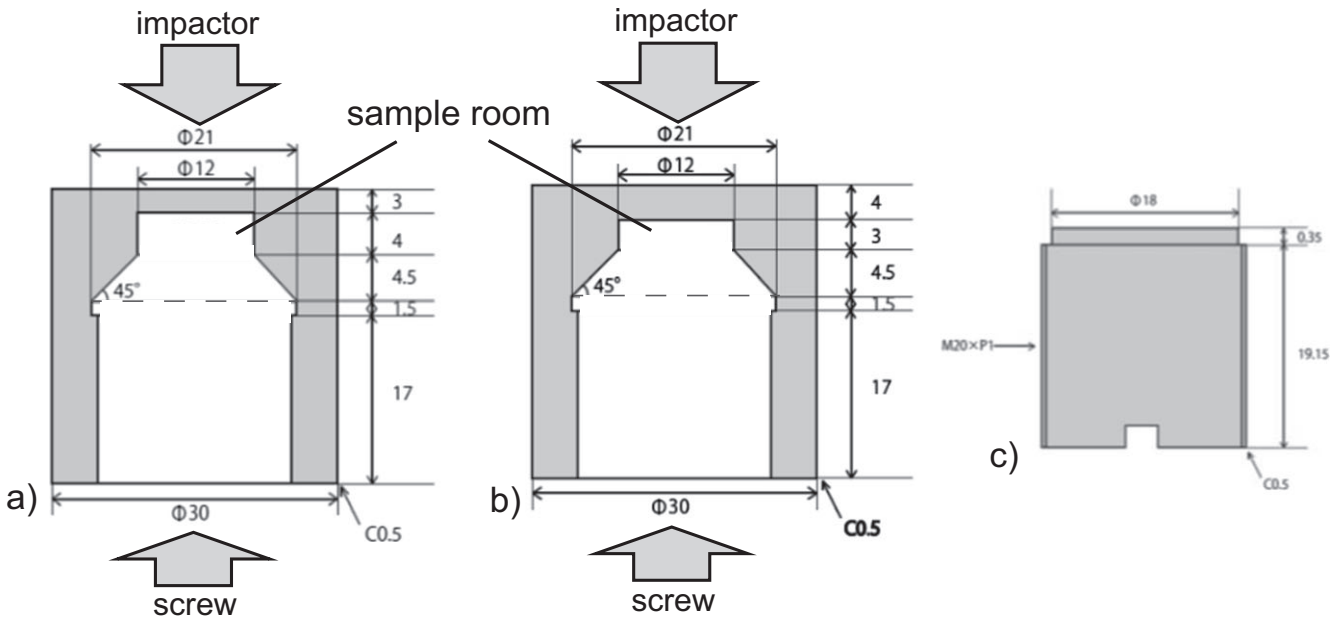

Fig. 1. Illustration of the stainless steel containers for our impact experiments. We used two types of containers. The container used for low-velocity impacts (a) has a 3 mm thick wall in front of the sample space on the impactor side. The other container is for high-velocity impacts (b) and has a 4 mm thick wall to avoid rupture of the container. The sample space is sealed by the stainless steel screw (c). The unit of the numbers in the illustrations is mm.

These collisions generate a shock wave in the container that propagates in the sample space of the target container and then reflects back from the back side of the sample space. In the experiments, we attempted to make a single shock alteration for the OSPB samples until the rarefaction wave catches up with the shock wave. The usage of a single shock method is desirable because organic matter on planetary bodies would usually be expected to experience a single shock following an impact. In our experimental setup, the thickness of an isobaric core within the sample is estimated to be ~2 mm. To avoid multiple shock waves, we designed the thickness of the sample space to be 3 mm and used the samples within the thickness of 2 mm from the front side of the sample space for the detailed analyses mentioned later.

After introducing the sample into the sample space within the stainless steel container, it was set in a target chamber downstream of the propellant gun. Prior to the impact, the target chamber was evacuated to <1 Torr with a mechanical and blower pump. After a collision, the impacted container was collected, and the back side of the container was carefully removed with a lathe machine. We collected shocked sample from the center region of the sample room to avoid the effect of the metallic wall on the recovered sample. The collected samples were treated with 2 mL of 50% HF solution at 80 °C to remove quartz grains in Teflon jars for 2 h. The Teflon jars containing the samples were ultrasonically agitated for 30 min. This procedure was repeated three times in all. After the agitation, the samples were reacted with 50% HF solution for 18 h, and then the HF solutions were dried at 80 °C. The residues were rinsed with pure water and then dried. The rinse of the residue was repeated three times in all. Together with the shock recovery samples, we performed this treatment for unshocked samples to evaluate the effect of the treatment. As a control, we confirmed that this treatment produced no significant effect on the composition and structure of unshocked OSPBs within the errors of the Raman measurements and in terms of characteristics of the IR spectra (see Table S1 and Fig. S1 of supporting information for Raman data and IR spectra of the untreated samples, respectively).

The peak shock pressures achieved in the experiments were calculated with the impedance matching method using a planner impact approximation (Melosh 1989). The Hugenoit parameters used in the study are derived from Marsh (1980) and summarized in Table 2. The peak shock temperatures, or Hugenoit temperatures, were calculated with the relationship obtained by the Rankine-Hugoniot equation and thermodynamic relations given by Sugita et al. (2003). Table 1 summarizes the target properties and impact conditions of the impact experiments. In the present study, we subjected each type of OSPBs to approximately four levels of peak shock pressure—namely 2–3, 3–5, 7–8,

Table 2. Hugenoit parameters used in the present study. Data are derived from Marsh (1980).

	Density (kg m^{-3})	C_0 (km s^{-1})	S
Quartz (SiO_2)	2204	1.88	1.41
Al 6061 (impactor)	2703	5.35	1.34
SUS 304 (impactor and target holder)	7890	4.58	1.49

and 11–12 GPa (Table 1)—to study changes in the composition and structure of the materials as a function of peak shock pressure and temperature.

Analysis

The present study performed IR spectroscopy, Raman spectroscopy, and elemental and isotopic analyses on the shock recovery OSPBs to investigate changes in their structures and compositions resulting from hypervelocity impact.

IR Analysis

The IR spectroscopy was performed with a Fourier transform infrared (FT-IR) spectrometer (Frontier IR/NIR; PerkinElmer) at the University of Tokyo. The measured wave number range was 800–4000 cm^{-1} with a resolution of 1 cm^{-1}. Scans were averaged over a 5 min period. We employed the KBr tablet method to obtain IR spectra of OSPBs, in which a well-mixed powder of OSPBs and KBr (OSPBs/KBr = ~1/2000) was pressed at ~24 MPa to make a tablet. We used a KBr tablet without OSPBs as a reference to obtain the transmittance. Absorptions due to water vapor and CO_2 gas in the ambient atmosphere were calibrated with commercial software (Atmospheric Vapor Compensation™; PerkinElmer, Inc.).

Raman Spectroscopy

Raman spectroscopy was carried out for OSPBs with a Laser Raman spectrometer (NRS-3100, JASCO) at the University of Tokyo. The OSPBs were set on a precleaned slide glass and analyzed in air. The exciting wavelength of the Nd:Yag laser was 532 nm, and the measured wave number range was 300–4000 cm^{-1} with a resolution of 0.5 cm^{-1}. The Raman spectrometer was equipped with a microscope that allowed us to focus the laser beam onto the samples. A typical diameter of the laser spots on the OSPBs was about 2 μm, and the laser power density was ~1–4 mW μm^{-2}.

The present study focused on the G ("graphite") and D ("disordered") bands near 1580 and 1350 cm^{-1}, respectively, because the structural order of benzene rings contained in organic matter can be examined by their band widths (Γ_G and Γ_D), peak wave numbers (ω_G and ω_D), and the ratio of their peak intensities (I_D/I_G) (e.g., Ferrari and Robertson 2001; Busemann et al. 2007; Quirico et al. [2014] and references therein). For instance, both Γ_G and Γ_D broaden with increasing disorder of the structure of benzene rings contained in organic matter. With increasing disorder, ω_G also shifts to higher wave numbers due to the appearance of another band (the D′ band). The I_D/I_G dramatically decreases when organic matter contains ordered structures, i.e., graphitization.

In the present study, we obtained these parameters by fitting the measured Raman spectra with two Lorenz functions using commercial software (Origin2015, OriginLab). Organic matter often produces fluorescence when it is illuminated by laser irradiation and this can result in a sloping continuum under the G and D bands. In the present study, we assumed a linear function connecting two points at 900 and 1900 cm^{-1} to represent the background fluorescence and removed the data with an irregular-shaped background from the analysis. For each sample, Raman spectra were obtained at six different points on the sample, and the averaged Γ_G, Γ_D, ω_G, ω_D, and I_D/I_G were obtained. The errors of the obtained data were derived from the standard deviation of the measurements at these six points. The nominal laser irradiation time was 5 s in our analyses (the Raman parameters for different laser irradiation times of 2 and 20 s are compared in Table S1). The results show that the laser-induced thermal alteration of the samples is insignificant compared with the range of measurement error.

Elemental and Isotopic Analyses

A modified online version of the Finnigan Delta Plus XP isotope-ratio mass spectrometer coupled to a Flash EA1112 elemental analyzer through a ConFlo III interface at JASMTEC (Ogawa et al. 2010) was employed to measure the C/N ratio and carbon and nitrogen isotopic compositions of our OSPBs. For these analyses, ~0.06 mg of OSPBs was loaded into tin cups and then introduced into the sample chamber of the mass spectrometer system. Using calibrated ion currents with m/z 44, 45, and 46 (CO_2^+) and m/z 28, 29, and 30 (N_2^+) in the mass spectrometer, C/N mass ratios of OSPBs were determined. Carbon isotopic composition is expressed using δ notation with respect to the VPDB standard: $\delta^{13}C$ (‰) = $(^{13}R_{sample}/^{13}R_{standard} - 1) \times 1000$, where ^{13}R is $^{13}C/^{12}C$ ratio. Nitrogen isotopic compositions are also expressed using δ notation with respect to the standard of the air nitrogen: $\delta^{15}N$ (‰) = $(^{15}R_{sample}/^{15}R_{standard} - 1) \times 1000$, where ^{15}R is $^{15}N/^{14}N$ ratio. The analytical precision of $\delta^{13}C$ and $\delta^{15}N$ values was evaluated based on repeated

measurements (n = 5–14) of standard materials (L-tyrosine) (Tayasu et al. 2011). The errors of $\delta^{13}C$ and $\delta^{15}N$ values are derived from the standard deviations of the $\delta^{13}C$ and $\delta^{15}N$ values for the standard materials, which were measured in the same analysis session of the mass spectrometer. The errors of $\delta^{13}C$ and $\delta^{15}N$ values for preshocked OSPBs are 0.64‰ and 0.33‰, respectively; those of postshocked OSPBs are 0.17‰ and 0.68‰, respectively.

RESULTS

Infrared Spectra

Figure 2 shows IR spectra of pre- and postshocked OSPBs for different peak shock pressures. The preshocked OSPBs contain the characteristics of hydrogen-related bonds, such as N-H and/or O-H bonds (2800–3600 cm^{-1}), and C-H bonds (2900 cm^{-1}); oxygen-related bonds, such as C=O bonds (1700 cm^{-1}), O-H bonds (1400 cm^{-1}), C-O bonds (1100 cm^{-1}); and unsaturated bonds, such as olefinic C=C and/or C=N double bonds (1600–1670 cm^{-1}), and aromatic C=C bonds (1580 cm^{-1}). These results are consistent with the previous results of IR analysis of OSPBs formed through polymerization of formaldehyde (Cody et al. 2011; Kebukawa et al. 2013). Together with NMR and XANES analyses, they suggest that these organic materials consist of poly-olefin containing aromatic moieties terminated with polar functional groups, such as –OH and $–NH_2$ bonds (Cody et al. 2011; Kebukawa et al. 2013).

A comparison of IR spectra of preshocked OSPBs shows that low-NH_3 OSPBs formed at 130 and 200 °C contain less C=N (and C=C) bonds (1600 cm^{-1}) and more C=O bonds (1700 cm^{-1}), compared to the high-NH_3 OSPBs formed at 130 and 200 °C (Fig. 2). This suggests that high-NH_3 OSPBs tend to contain more nitrogen and less oxygen, a conclusion consistent with the results of our elemental analyses (see below). Comparing the formation temperature, the OSPBs formed at 200 °C show strong absorption due to C-O bonds at ~1100 cm^{-1}, while the OSPBs formed at 130 °C do not (Fig. 2). The presence of more C-O bonds in the OSPBs formed at 200 °C may reflect that polymerization and dehydration proceed more effectively at 200 °C during the formation of OSPBs (Kebukawa et al. 2013).

Figure 2 shows that the overall IR spectra of samples subjected to peak shock pressures of 2–5 GPa are similar to those of preshocked OSPBs, suggesting that the molar structure of OSPBs does not change significantly upon an impact. One exception is an increase in absorption by C-O bonds at 1100 cm^{-1} for the OSPBs formed at 130 °C (Fig. 2). This may be caused by dehydration reactions, such as esterification, forming C-O bonds from C-H and COOH bonds.

In contrast, at peak shock pressures ≥7–8 GPa, pre-existing absorptions due to functional groups containing N-H, C-H, C=N, and C=O bonds disappear in the IR spectra of postshocked OSPBs (Fig. 2). The disappearance of absorption in the shocked OSPBs occurs independent of the initial composition and structure of the original unshocked OSPBs (Figs. 2a–d).

Raman Spectra

Figure 3 shows typical Raman spectra of pre- and postshocked OSPBs for different peak pressures. This figure shows the occurrence of shifts in the G bands to higher wave numbers for higher levels of peak shock pressure, e.g., ≥7–8 GPa. The features of both the G and D bands also become sharper for higher levels of peak shock pressure. These results are confirmed in relationships between ω_G and Γ_G (Fig. 4) and between Γ_G and Γ_D (Fig. 5). The measured Raman spectral parameters are summarized in Table 3.

Figure 4 shows that both increases in ω_G and decreases in Γ_G are observed in postshocked OSPBs for peak shock pressures above 7–8 GPa, although the values for preshocked and weakly shocked (shock pressures ≤~5 GPa) OSPBs range widely at ω_G of 1565–1580 cm^{-1} and Γ_G of 110–150 cm^{-1}. Despite the difference in the composition of starting solution and formation temperature, the metamorphic trend of ω_G and Γ_G is common among the four types of OSPBs (Fig. 4).

Figure 5 shows the relationship between Γ_G and Γ_D for the pre- and postshocked OSPBs. This figure shows that both Γ_G and Γ_D decrease at peak pressures above 7–8 GPa, although the values for preshocked and weakly shocked OSPBs vary over ranges for Γ_G of 110–150 cm^{-1} and Γ_D of 280–380 cm^{-1}. These results indicate that the structure of OSPBs does not change significantly at peak pressures <~5 GPa, but it abruptly changes at peak pressures ≥7–8 GPa. The result of shock pressure of 7–8 GPa for low-NH_3 OSPBs (light gray circle) exhibits lower Γ_G and Γ_D than the results of 7–8 GPa for the other OSPBs (Fig. 5). This is likely because the low-NH_3 OSPBs experienced a higher shock pressure (~8.5 GPa) than the others (6.9–7.1 GPa).

Both the increase in ω_G and decreases in Γ_G and Γ_D with increasing shock pressure suggest a decrease in disordered structures in the OSPBs upon a shock at ≥7–8 GPa. According to previous studies (e.g., Ferrari and Robertson 2001; Busemann et al. 2007), the peak widths of both the D and G bands become narrower with decreasing disorder of carbon in organic matter. In addition, decreasing disorder of carbon in organic

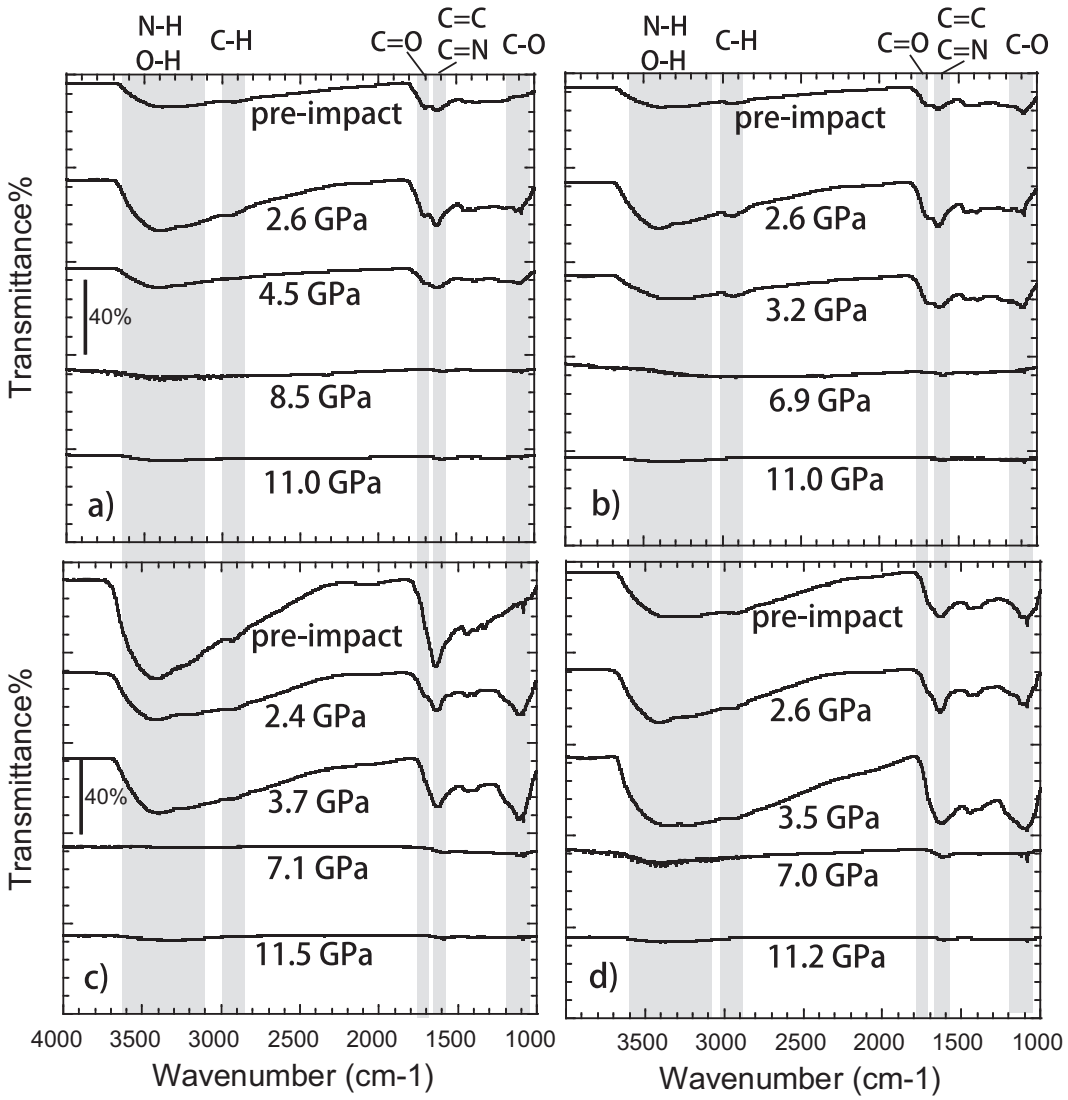

Fig. 2. Infrared spectra of OSPBs before and after impacts: (a) low-NH_3 OSPBs formed at 130 °C; (b) low-NH_3 OSPBs formed at 200 °C; (c) high-NH_3 OSPBs formed at 130 °C; and (d) high-NH_3 OSPBs formed at 200 °C. Intensities are offset vertically for clarity. The peak shock pressures of the impacts are also shown in the figures.

matter can cause other bands to appear (e.g., the D′ band at ~1620 cm^{-1}), leading to an apparent shift in the G band to higher wave numbers (e.g., Busemann et al. 2007). Thus, our Raman spectroscopy results show that a decrease in disorder of the carbon in the OSPBs structure occurs upon shock pressure ≥7–8 GPa. The previous studies on characterization of thermally altered organic matter (e.g., Ferrari and Robertson 2001; Busemann et al. 2007) suggest that a decrease in disorder in thermally altered organic matter is caused by formation of nano-crystalline graphite due to heat. Formation of nanocrystalline graphite would be caused by dehydration of the organic matter. Thus, the conclusion of a decrease in disorder in the highly shocked OSPBs is consistent with the results of IR spectra of disappearance of pre-existing H-related bonds, such as C-H and N-H bonds (Fig. 2).

Despite decreasing disordered structures in the OSPBs, graphitic carbon would not be predominant in the OSPBs in this shock pressure range (i.e., ≥7–8 GPa), possibly due to a short period of shock in our experiments. Figure 6 shows the relationship between I_D/I_G and Γ_D obtained by the Raman spectroscopy for pre- and postshocked OSPBs. Formation of the graphitic carbon structure in organic matter should result in a sharp decrease in I_D/I_G (e.g., Busemann et al. 2007). Nevertheless, Fig. 6 shows that the I_D/I_G ratio does not decrease upon shock. Although graphitic carbon does not appear to be predominant in our shocked samples, we

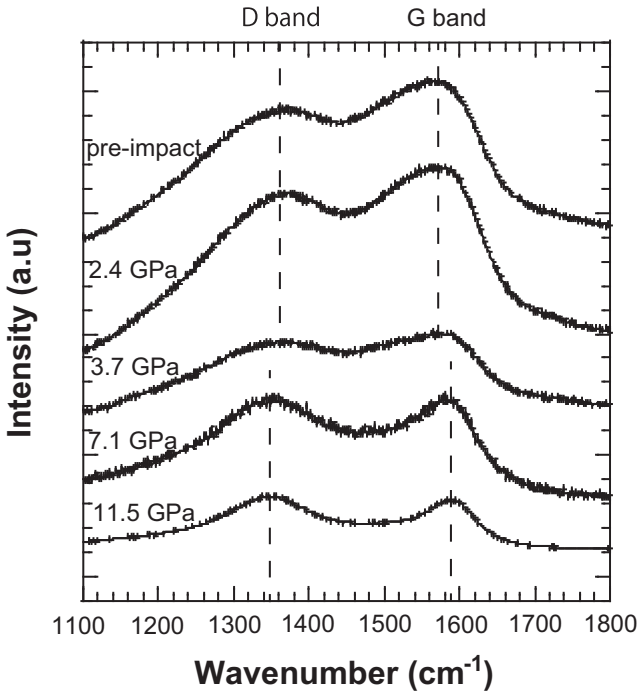

Fig. 3. Typical Raman spectra of pre- and postshocked high-NH_3 OSPBs formed at 130 °C. Intensities are offset vertically for clarity. The peak shock pressures of the impacts are also shown in the figures.

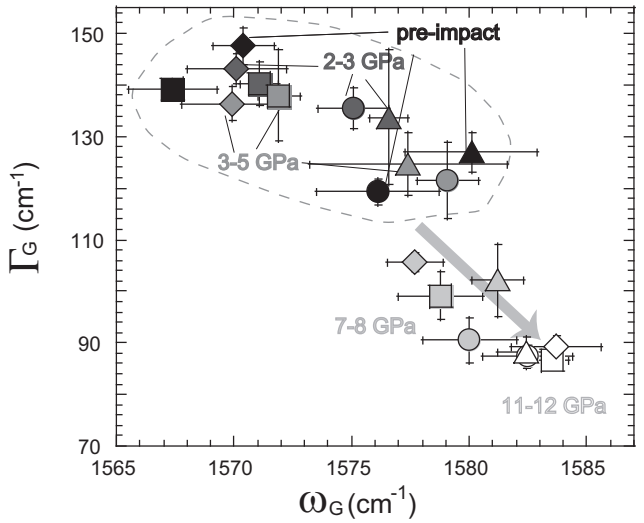

Fig. 4. The relationship between the Raman spectral parameters ω_G and Γ_G for OSPBs for different peak shock pressures (color of the data points: black = preimpact; dark gray = 2–3 GPa; gray = 3–5 GPa; light gray = 7–8 GPa; and white = 11–12 GPa). Circles and triangles represent the results of low-NH_3 OSPBs that were produced at 130 and 200 °C, respectively. Squares and diamonds represent the results of high-NH_3 OSPBs that were produced at 130 and 200 °C, respectively. The area surrounded by the broken line indicates the range of ω_G and Γ_G for preshocked and weakly shocked OSPBs. The gray arrow represents the impact-induced metamorphic pathway at shock pressures ≥7–8 GPa.

cannot rule out the local presence of graphitic carbon in the OSPBs. This is because graphene oxide films containing local graphene exhibit relatively high I_D/I_G ratios ($I_D/I_G \sim 1$) (e.g., Yang et al. 2009; Erickson et al. 2010), which are comparable to those of the OSPBs for shock pressure of 11–12 GPa in the present study. Thus, our results suggest that carbonization would be the plausible process of impact-induced alteration of the OSPBs at peak pressures of 7–12 GPa, although the formation of local graphite structures cannot be ruled out.

Elemental and Isotopic Compositions

The measured C/N ratios and isotopic compositions of carbon and nitrogen for pre- and postimpact OSPBs are summarized in Table 3. Figure 7 shows the variation in the C/N ratio contained in pre- and postshocked OSPBs as a function of peak shock pressure. Before the impacts, the C/N ratios of low-NH_3 OSPBs are about twice those of high-NH_3 OSPBs (Fig. 7). The high contents of nitrogen in the preshocked, high-NH_3 OSPBs are consistent with the results of IR spectra of the presence of large absorptions due to N-H and C=N bonds (Fig. 2). On the other hand, there is no

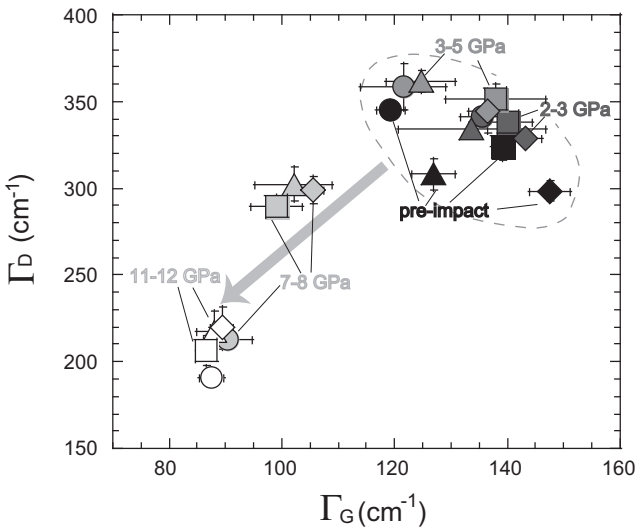

Fig. 5. The relationship between Raman spectral parameters Γ_G and Γ_D for OSPBs for different peak shock pressures. Symbols, colors, broken line area, and arrow have the same meanings as in Fig. 4.

difference in the C/N ratio regarding the formation temperature of OSPBs, if the NH_3 contents of the starting solutions are same.

Table 3. Summary of the measured data of ω_G, ω_D, Γ_G, Γ_D, I_D/I_G ratio, C/N ratio, $\delta^{13}C$, and $\delta^{15}N$ values of pre- and postimpact OSPBs. The term "u.m" in $\delta^{15}N$ represents "unmeasurable" due to low nitrogen contents. For the errors in the elemental and isotope analyses, see the main text.

OSPBs	Shock pressure (GPa)	ω_G (cm^{-1})	ω_D (cm^{-1})	Γ_G (cm^{-1})	Γ_D (cm^{-1})	I_D/I_G ratio	C/N ratio	$\delta^{13}C$ (‰)	$\delta^{15}N$ (‰)
Low-NH_3 130 °C	0	1576.1 ± 2.6	1357.5 ± 4.2	119.3 ± 2.5	345.3 ± 5.5	1.14 ± 0.06	9.8	−24.5	0.6
	2.61	1575.1 ± 1.5	1361.3 ± 2.9	135.5 ± 3.9	341.1 ± 5.0	1.21 ± 0.02	9.8	−25.9	−1.0
	4.49	1579.1 ± 1.3	1359.9 ± 2.5	121.5 ± 7.5	358.5 ± 13.1	1.21 ± 0.09	10.7	−25.8	−2.0
	8.53	1580.0 ± 2.0	1346.6 ± 2.7	90.5 ± 4.3	213.1 ± 5.5	1.09 ± 0.03	25.0	−25.9	−1.3
	11.05	1582.5 ± 1.9	1344.9 ± 1.9	87.5 ± 2.1	191.1 ± 5.4	1.14 ± 0.04	37.5	−26.4	u.m
Low-NH_3 200 °C	0	1580.1 ± 2.8	1359.8 ± 0.8	126.9 ± 3.9	308.2 ± 8.9	1.17 ± 0.10	9.9	−23.1	2.2
	2.57	1576.6 ± 0.8	1360.5 ± 1.9	132.1 ± 13.0	334.4 ± 4.1	1.29 ± 0.06	10.2	−25.7	−0.8
	3.17	1577.4 ± 4.2	1362.9 ± 1.5	124.7 ± 6.1	361.7 ± 6.0	1.20 ± 0.08	11.1	−25.7	−0.7
	6.93	1581.2 ± 1.1	1354.8 ± 2.9	102.1 ± 6.9	302.4 ± 9.5	1.12 ± 0.05	13.0	−25.7	−0.5
	10.98	1582.4 ± 1.2	1344.3 ± 1.5	88.1 ± 3.1	217.6 ± 11.2	1.10 ± 0.05	25.2	−25.7	u.m
High-NH_3 130 °C	0	1567.4 ± 1.9	1349.8 ± 1.2	139.1 ± 1.9	323.7 ± 7.7	1.27 ± 0.04	4.2	−21.2	10.0
	2.42	1571.1 ± 0.8	1356.7 ± 3.1	140.2 ± 4.2	337.9 ± 4.0	1.22 ± 0.05	4.7	−25.3	9.4
	4.71	1571.9 ± 0.9	1354.8 ± 2.5	137.9 ± 8.8	351.6 ± 8.1	1.31 ± 0.05	5.0	−26.4	9.9
	7.10	1578.8 ± 1.8	1350.1 ± 1.2	99.1 ± 4.6	289.6 ± 6.5	1.24 ± 0.03	8.5	−26.5	10.0
	11.49	1583.5 ± 0.7	1345.7 ± 1.1	86.6 ± 1.6	206.2 ± 8.7	1.13 ± 0.03	18.5	−26.1	u.m
High-NH_3 200 °C	0	1570.4 ± 1.3	1355.2 ± 1.3	147.5 ± 3.6	298.3 ± 5.8	1.33 ± 0.04	4.6	−21.6	10.7
	2.55	1569.3 ± 2.1	1355.0 ± 1.7	143.2 ± 2.9	328.5 ± 4.7	1.25 ± 0.03	5.2	−24.8	7.4
	3.51	1569.9 ± 2.1	1357.1 ± 1.2	136.4 ± 3.2	344.2 ± 12.5	1.22 ± 0.12	–	–	–
	6.95	1577.7 ± 1.2	1351.4 ± 1.4	105.6 ± 1.9	299.1 ± 7.7	1.20 ± 0.04	8.8	−25.8	9.6
	11.16	1583.7 ± 1.9	1347.5 ± 1.2	89.4 ± 2.0	219.4 ± 12.5	1.14 ± 0.04	15.4	−26.1	u.m

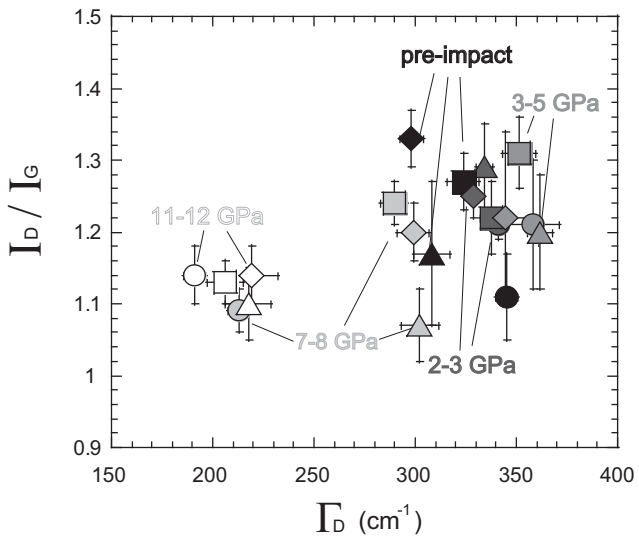

Fig. 6. The relationship between Raman spectral parameters I_D/I_G and Γ_D for OSPBs for different peak shock pressures. Symbols and colors have the same meanings as in Fig. 4.

Figure 7 shows that even after an impact, the C/N ratio of OSPBs remains almost constant for peak pressures <~5 GPa. However, the C/N ratio increases with peak pressure above 7–8 GPa (Fig. 7). The C/N ratios after an impact with peak pressures of 11–12 GPa reach 2–4 times the preshocked values (Fig. 7). These results suggest that nitrogen contained in OSPBs as $-NH_2$ and –NH tends to preferentially degas upon shock compared with carbon, whereas a fraction of carbon contained in the preshocked OSPBs remains in the solid phase through carbonization upon shock.

Figure 8 shows the variations of isotopic compositions of carbon ($\delta^{13}C$) and nitrogen ($\delta^{15}N$) contained in pre- and postshocked OSPBs as a function of peak pressure. Compared with preshocked OSPBs, $\delta^{13}C$ and $\delta^{15}N$ values of postshocked OSPBs appear to decrease even for peak pressure at 2 GPa. This might happen because low-molecular-weight organic compounds with very high $\delta^{13}C$ and $\delta^{15}N$ values could be desorbed from the surface of the OSPBs upon a shock. In fact, our results of nitrogen isotopic analyses for the liquid residues after the organic synthesis experiments show that $\delta^{15}N$ values of low-molecular-weight organic compounds remaining in the liquid are high, namely $\delta^{15}N = 20.7‰$ for high-NH_3 OSPBs formed at 130 °C and $\delta^{15}N = -0.2‰$ for low-NH_3 OSPBs formed at 130 °C. Unlike the C/N ratio of postshocked OSPBs, $\delta^{13}C$ and $\delta^{15}N$ values do not change significantly within ±2‰ even for high peak pressures ≥7–8 GPa. This suggests small or no isotopic fractionation of carbon and nitrogen in the transition in the structure and composition of OSPBs upon shock at peak pressure of 7–8 GPa.

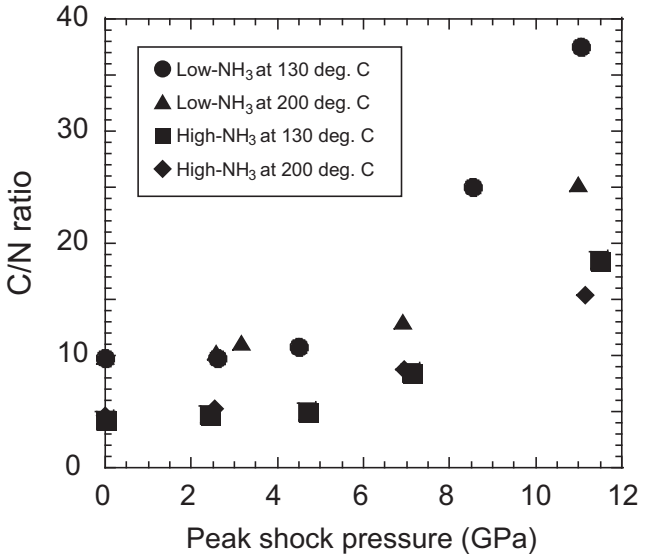

Fig. 7. Molar C/N ratios of pre- and postshocked OSPBs as a function of peak shock pressure. The C/N ratios increase significantly at peak shock pressure ≥7–8 GPa, suggesting a loss of $-NH_2$ bonds within the OSPBs upon shock.

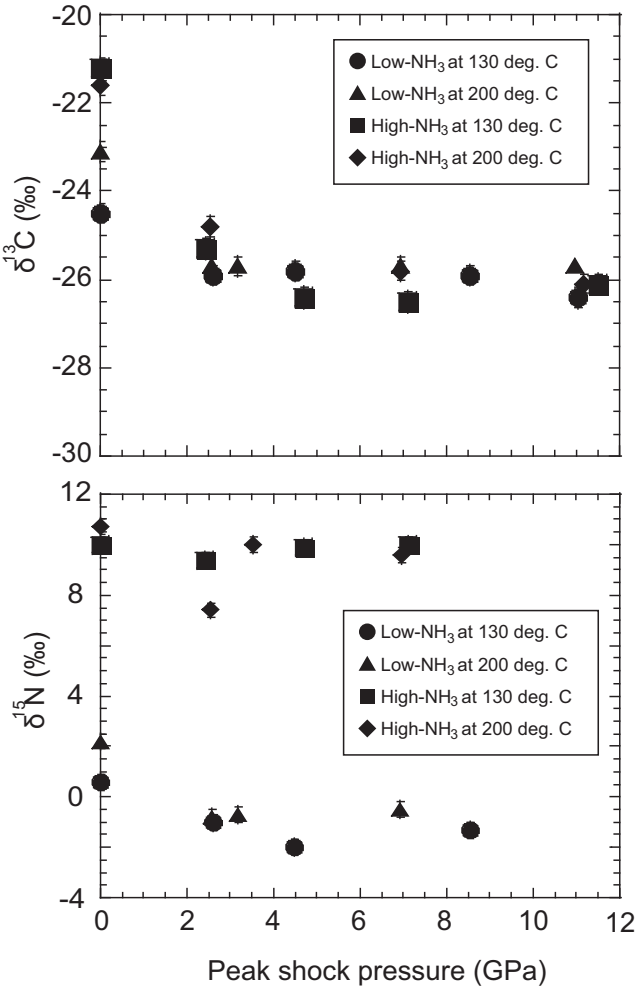

Fig. 8. $\delta^{13}C$ and $\delta^{15}N$ vales of pre- and postshocked OSPBs as a function of peak shock pressure. Changes in $\delta^{13}C$ and $\delta^{15}N$ values between pre- and postshocked OSPBs may be due to desorption of highly volatile organic compounds onto the OSPBs upon shock. However, the C/N ratios change at shock pressure ≥7–8 GPa (Fig. 7). $\delta^{13}C$ and $\delta^{15}N$ values remain almost constant, implying homogeneity of isotopic composition of OSPBs.

DISCUSSION

In this section, we first discuss the possible mechanism of impact-induced alterations of OSPBs as a function of peak pressure and temperature as suggested by our analytical results. Then, we discuss shock pressures and impact velocities achieved in meteorite samples by comparing our Raman spectroscopy results with the spectra of carbonaceous meteorites. Finally, we briefly discuss the implications of our results for the methodology and conditions for intact capture of organic compounds in spacecraft missions to icy satellites and C-type asteroids.

Mechanism of Impact-Induced Alteration

Our results show that impact-induced alteration of OSPBs is mainly controlled by the peak pressure and temperature created by the impact and is less dependent on the initial structure and composition of OSPBs (Fig. 9). Our IR spectroscopy results (Fig. 2) suggest that at peak pressure of 2–5 GPa and a Hugenoit temperature of 200–350 °C, some hydrolysis and consequent polymerization would proceed upon an impact for OSPBs formed at 130 °C (Fig. 9), possibly including esterification that forms C–O bonds in OSPBs (Fig. 2). For OSPBs formed at 200 °C, no significant change in the composition and structure of OSPBs is observed (Fig. 9). This is possibly because hydrolysis and polymerization have already proceeded in OSPBs during the formation of the OSPBs at 200 °C.

Our results of Figs. 2–6 show that at peak pressures of 7–8 GPa and Hugenoit temperatures of 400–550 °C, remarkable destruction of H-related and N-related bonds and dehydration take place upon a shock (Fig. 9). This is confirmed by a change in the elemental compositions of C/N ratio, although isotopic fractionation does not occur effectively ($\delta^{13}C$ and $\delta^{15}N$ variations within ±2‰) (Fig. 7). The Raman spectroscopy results suggest that at these pressures and temperatures, carbonization proceeds effectively, possibly through Robinson annulation, a process in which a ketone and methyl vinyl ketone form an unsaturated ketone in a cyclohexene ring (e.g., Rapson and Robinson 1935).

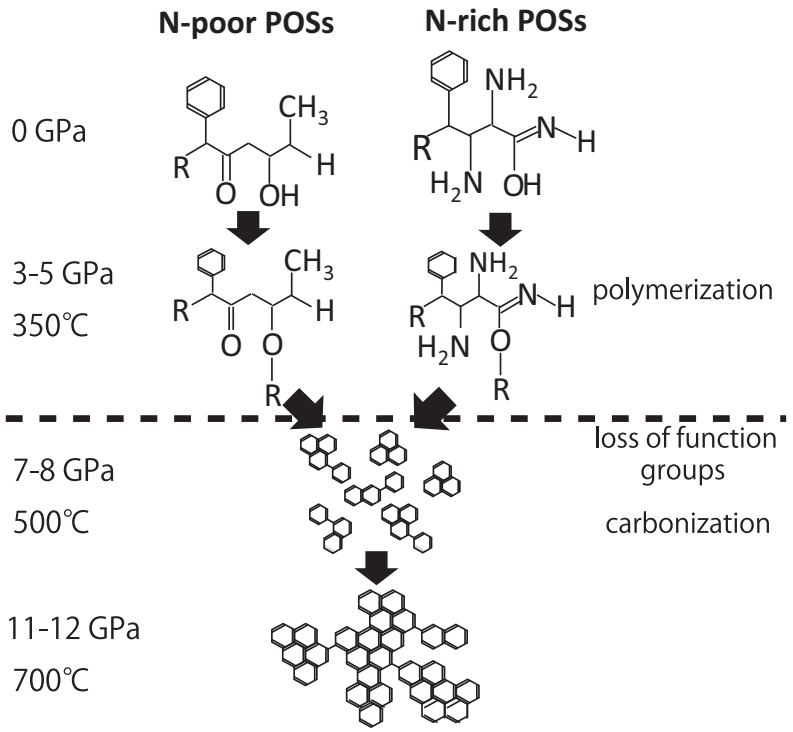

Fig. 9. The proposed mechanism of shock-induced alteration of OSPBs. The chemical structure of preshocked OSPBs is hypothetical and partly based on Cody et al. (2011) and Kebukawa et al. (2013). Dehydration and polymerization of OSPBs can occur upon a shock with peak pressure of 3–5 GPa and temperature of ~350 °C. The threshold peak pressure and temperature for shock-induced alteration (loss of function group and carbonization) are around 7–8 GPa and 500 °C, respectively. Above these thresholds, the initial structure and composition of OSPBs are largely lost due to shock heating.

Previous results of impact experiments show that dehydration and polymerization of aromatic hydrocarbons proceeds at peak pressures of 10–20 GPa and Hugenoit temperatures of 400–700 °C (Mimura et al. 2005). Their reported temperature threshold for dehydration is in agreement with our results (400–550 °C), although the achieved pressure of the previous study is higher than that of our experiments (7–8 GPa). In static heating of simple aromatic hydrocarbons, similar dehydration and carbonization occur at ~500 °C and 9 MPa (Greinke and Lewis 1984). Again, the temperature condition for dehydration in static heating is consistent with that of our experiments. These comparisons imply that temperature may be a major controlling parameter for dehydration and carbonization of organic compounds, at least in the pressure range up to ~20 GPa.

Comparison with IOM in Carbonaceous Chondrites

We compare thermal alteration of organic matter by shock heating with those by static heating in the Raman parameters on the basis of the framework defined by Ferrari and Robertson (2001). Figure 10 compares our Raman spectroscopy results with those of statically heated tetrahedral amorphous carbon (ta-C:H) (Ferrari and Robertson 2001), coals (Quirico et al. 2005), and IOMs of carbonaceous chondrites (Quirico et al. 2014). Our OSPBs, ta-C:H, coals, and chondritic IOMs appear to be chemically distinct, as evidenced by the fact that the initial ω_G and Γ_G of organic matter are different among these. Nevertheless, this figure shows that the trend of thermal alteration by shock heating is similar to those of static heating—high-temperature alteration results in higher values for ω_G and lower values for Γ_G in this diagram regardless of the initial composition and structure of the material (Fig. 10). We suggest that it would be difficult to distinguish the heating process of organic matter, i.e., static or dynamic, solely based on Raman spectroscopy.

The range of ω_G and Γ_G for highly shocked OSPBs lies below than those of carbonaceous chondrites or natural coals (Fig. 10). These ω_G and Γ_G for highly shocked OSPBs are rather consistent with those of glassy carbon (ω_G = ~60 cm^{-1} and Γ_G = 1580–1590 cm^{-1}) (e.g., McCulloch et al. 1994). Glassy carbon is usually formed by restricted devolatilization of a carbonaceous precursor upon high-temperature heating (e.g., ~1600 °C) (e.g., McCulloch et al. 1994). Thus, a possible interpretation for the difference in ω_G and Γ_G between high-shocked OSPBs

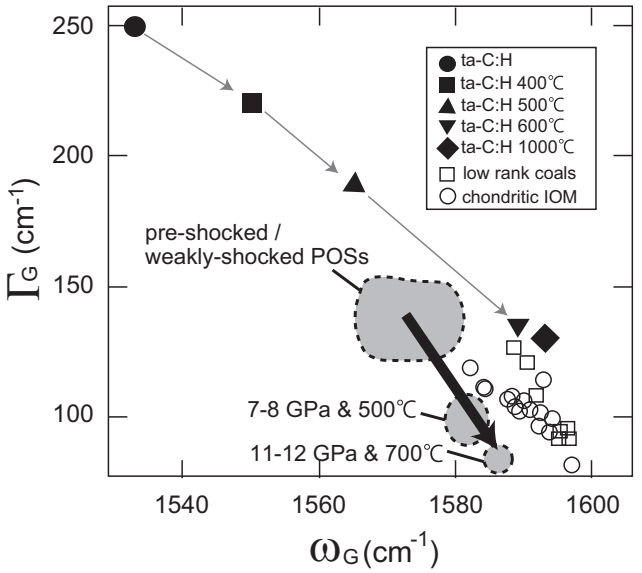

Fig. 10. A comparison of shock and static heating in Raman spectral parameters of ω_G and Γ_G. The results of static heating are derived from the previous studies of tetrahedral amorphous carbon (ta-C:H) (532 nm excitation) (Ferrari and Robertson 2001), coal (514 nm excitation) (Quirico et al. 2005), and IOM of carbonaceous chondrites (514 nm excitation) (Quirico et al. 2014). The metamorphic trend of organic matter by shock heating is similar to those by static heating in this diagram, although the gradient obtained by the present study is steeper than those of the previous studies of static heating. The black and gray arrows denote the trend of Raman parameter change of shock and static heating, respectively.

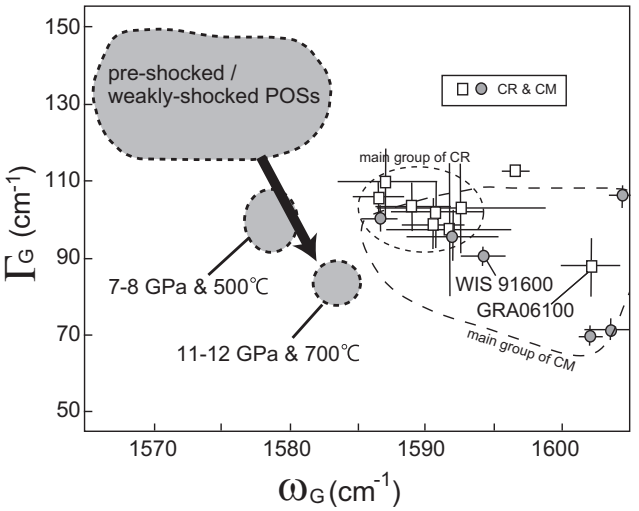

Fig. 11. A comparison of the Raman spectral parameters ω_G and Γ_G for OSPBs in the present study and IOM in carbonaceous chondrites (514 nm excitation) given by Briani et al. (2013). CM chondrite of WIS 91600 and CR chondrite of GRA 06100 are suggested to have been thermally metamorphosed by an impact (Yabuta et al. 2010; Briani et al. 2013; Quirico et al. 2014).

and chondritic IOMs would be a difference in a degree of restriction of devolatilization during heating, implying that our OSPBs may have experienced more restricted devolatilization than natural chondrites.

Figure 11 compares our results for the OSPBs' Raman parameters ω_G and Γ_G with those of carbonaceous chondrites (Briani et al. 2013). Previous studies have suggested that some meteorites, such as WIS 91600 (CM2) and GRA 06100 (CR), have experienced short-duration thermal metamorphism, plausibly caused by an impact (Yabuta et al. 2010; Briani et al. 2013; Quirico et al. 2014). The Raman spectra of IOM contained in PCA 91008 and GRA 06100 shows shifts in ω_G and Γ_G distinct those of unmetamorphosed CR meteorites, whereas those of WIS 91600 are within the range of unmetamorphosed CM meteorites (Briani et al. 2013; Quirico et al. 2014).

Our experimental results indicate that a shift in ω_G and Γ_G in preshocked/weakly shocked OSPBs occurs at peak pressures >7–8 GPa and Hugenoit temperatures >400–550 °C. The chemical structure of our OSPBs is not identical to those of chondritic IOMs. Nevertheless, previous studies suggest that IOMs and OSPBs (formaldehyde polymers) have common characteristics in functional groups (Cody et al. 2011; Kebukawa et al. 2013). Given that loss of functional groups, such as N-H and C-H bonds, would require energy that exceeds the bonding energy, we suggest that the abovementioned threshold peak pressure and temperature would be applicable to shock-induced alteration of IOMs. If the threshold is valid for meteoritic IOMs, we suggest that WIS 91600 has undergone a shock with peak pressure ≤~5 GPa and peak temperature <350 °C. Under such a low-shock condition, our results suggest that the original chemical and isotopic compositions and molar structure are largely preserved (Figs. 6–8). This is consistent with the previous results that the C/N ratio of IOM in WIS 91600 is similar to unmetamorphosed CM chondrites (Yabuta et al. 2010). The presence of C-H and C-O bonds in the IOM of WIS 91600 also supports our interpretation that this meteorite has experienced peak pressure and temperature <~5 GPa and ~350 °C, respectively. According to the impedance matching method (Melosh 1989), the peak pressure of ~5 GPa is achieved in an impact of a rocky projectile onto target with ~0.8 km s^{-1}. Since the average impact velocity in the Main Belt is estimated as ~5 km s^{-1} (Bottke et al. 1994), WIS 91600 would not have been located at the footprint of the impact on the meteorite parent body.

The Raman spectra of GRA 06100 show larger ω_G and lower Γ_G than those of unmetamorphosed CR meteorites (Briani et al. 2013). Our results of Fig. 4 show

that shock pressure (and temperature) of 7–8 GPa (and ~500 °C) results in a shift of 20–30 cm^{-1} in Γ_G and that of 5–10 cm^{-1} in ω_G, respectively, from the values for preshocked or weakly shocked OSPBs. Figure 11 shows that Γ_G and ω_G of GRA06100 exhibit a shift of 5–20 cm^{-1} in Γ_G and that of 10–30 cm^{-1} in ω_G, respectively, from the values of unmetamorphosed CR chondrites, which our results suggest can be explained by shifts due to shock pressure and temperature of 7–8 GPa and ~500 °C. Contrary to WIS 91600, our results suggest that GRA 06100 would have experienced peak shock temperature higher than 400 °C, suggesting that GRA 06100 was placed near the impact footprint and near the surface of its parent body. Our results show that under such a high shock condition, the disappearance of H-related functional groups due to dehydrogenation proceeds. However, Briani et al. (2013) reported the presence of H-related bonds, such as C-H bonds, in the IOM of GRA 06100. This implies that thermal alterations of IOM of GRA 06100 would not have proceeded in a single impact event but would have been a mixture of an impact and complex surface history, such as bombardments of solar winds.

Applications to Spacecraft Missions

Refractory organic matter is found in plume materials erupting from Enceladus (Postberg et al. 2011) (complex organic molecules with molecular weight in excess of 200 Da [Postberg et al. 2017]). Proposed spacecraft missions to Enceladus have been considered that would capture plume materials during flyby to Enceladus (Tsou et al. 2012; McKay et al. 2014; Sekine et al. 2014). The expected plume encounter velocity depends on the trajectory design of the mission, but can be as low as ~3 km s^{-1} (Tsou et al. 2012; Sekine et al. 2014). Given the threshold for shock-induced alteration of organic matter described in the present study, we propose the use of a low-impedance alloy, such as magnesium alloy (MgAZ31B: Mg 96%, Al 3%, Zn 1%), for such a capture instrument. For the magnesium alloy, the peak pressure and Hugenoit temperature achieved during the capture at an encounter velocity of ~3 km s^{-1} are estimated to be ~8 GPa and 300–350 °C, respectively, which is close to or less than the observed threshold for dehydration of OSPBs.

Given the similarity in reflectance spectra with carbonaceous chondrites, C-type asteroids are also highly likely to contain refractory organic matter. Considering the average impact velocity in the Main Belt of ~5 km s^{-1} (Bottke et al. 1994), organic matter near the surface would have been readily thermally altered or dissociated during impacts. However, asteroids are thought to be exposed to repeated destruction and reaccretion in the Main Belt, and less-cratered, fresh materials could be exposed on the surface. This is consistent with the presence of 3.4 μm absorption due to C-H bonds of organic matter on the surface of 24 Themis (Campins et al. 2010). Aliphatic organic compounds with C-H bonds are also observed on some regions of the surface of Ceres (De Sanctis et al. 2017). Our results show that C-H bonds contained in OSPBs are lost by an impact with Hugenoit temperature ≥400 °C, where their initial chemical compositions and molar structures are also lost. Thus, the present study suggests that asteroidal surfaces showing remote-sensing signatures of C-H bonds at 3.3–3.6 μm would be a promising indicator for the presence of less-altered organic matter (experience temperature in alteration <350 °C) suitable for collection of samples in Hayabusa2 and OSIRIS-REx missions.

CONCLUSIONS

The present study performs impact and recovery experiments to investigate systematically shock-induced alterations of OSPBs, using IR and Raman spectroscopy, and elemental and isotopic analyses. Based on the experimental results, we discuss the alteration mechanism of OSPBs as a function of the peak pressures and Hugenoit temperatures achieved as a result of the impacts. We can draw the following conclusions regarding the experimental results.

1. At peak pressures < 2–5 GPa and Hugenoit temperatures < 200–350 °C, the chemical structure of organic matter does not change significantly upon impact, although weak hydrolysis and polymerization can occur.
2. At peak pressures > 7–8 GPa and Hugenoit temperatures > 400–550 °C, dehydration and carbonization proceed significantly upon a shock. The shocked organic matter exhibits almost no absorptions due to functional groups, including those groups that contain hydrogen-related bonds. The chemical composition, including the C/N ratio, of the organic matter is also significantly changed due to shocks of this magnitude.
3. Compared with the previous studies of static heating of organic matter, it appears that temperature may be a major controlling factor for dehydration and carbonization of organic matter. The threshold temperature for the dehydration is ~ 400–500 °C.
4. The techniques of Raman and IR spectroscopy cannot distinguish between alteration due to dynamic heating by an impact and that due to static heating.

Our experimental results provide proxy indicators for interpreting the effect of shock alteration of organic

matter in carbonaceous chondrites. Our results also have implications for spacecraft missions to volatile-rich small bodies in the solar system. For instance, in asteroid sample-return missions such as Hayabusa2 and OSIRIS-REx, remote sensing of C-H bonds on the asteroidal surface can be a promising indicator for collecting organic matter that has experienced temperatures <350 °C and is likely to possess primordial chemical and isotopic compositions.

Acknowledgments—The two anonymous reviewers are deeply appreciated for their constructive comments. This work was supported by JSPS KAKENHI Grant Number JP16K13873 and JP26707024, MEXT KAKENHI Grant Number JP17H06456, and Grant in Aid from Astrobiology Center of the National Institutes of Natural Sciences (NINS).

Editorial Handling—Dr. Scott Sandford

REFERENCES

Alibert Y. and Mousis O. 2007. Formation of Titan in Saturn's subnebula: Constraints from Huygens probe measurements. *Astronomy & Astrophysics* 465:1051–1060.

Bernstein M. P., Sandford S. A., Allamandola L. J., Chang S., and Scharberg M. A. 1995. Organic compounds produced by photolysis of realistic interstellar and cometary ice analogs containing methanol. *The Astrophysical Journal* 454:327–344.

Bockelée-Morvan D., Crovisier J., Mumma M. J., and Weaver H. A. 2004. The composition of cometary volatiles. In *Comets II*, edited by Festou M. C., Keller H. U., and Weaver H. A. Tucson, Arizona: The University of Arizona Press. pp. 391–423.

Bottke W. F., Nolan M. C., Greenberg R., and Kolvoord A. 1994. Velocity distributions among colliding asteroids. *Icarus* 107:255–268.

Briani G., Quirico E., Gounelle M., Paulhiac-Pison M., Montagnac G., Beck P., Orthous-Daunay F.-R., Bonal L., Jacquet E., Kearsley A., and Russell S. S. 2013. Short duration thermal metamorphism in CR chondrites. *Geochimica et Cosmochimica Acta* 122:267–279.

Busemann H., Alexander C. M. O'D., and Nittler L. R. 2007. Characterization of insoluble organic matter in primitive meteorites by microRaman spectroscopy. *Meteoritics & Planetary Science* 42:1387–1416.

Campins H., Hargrove K., Pinilla-Alonso N., Howell E. S., Kelley M. S., Licandro J., Mothé-Diniz T., Fernández Y., and Ziffer J. 2010. Water ice and organics on the surface of the asteroid 24 Themis. *Nature* 464:1320–1321.

Cody G. D., Alexander C. M. O'D., Yabuta H., Kilcoyne A. L. D., Araki T., Ade H., Dera P., Fogel M., Militzer B., and Mysen B. O. 2008. Organic thermometry for chondritic parent bodies. *Earth and Planetary Science Letters* 272:446–455.

Cody G. D., Heying E., Alexander C. M. O'D., Nittler L. R., Kilcoyne A. L. D., Sandford S. A., and Stroud R. M. 2011. Establishing a molecular relationship between chondritic and cometary organic solids. *Proceedings of the National Academy of Sciences* 108:19,171–19,176.

Derenne S. and Robert F. 2010. Model of molecular structure of the insoluble organic matter isolated from Murchison meteorite. *Meteoritics & Planetary Science* 45:1461–1475.

De Sanctis M. C., Ammannito E., Raponi A., Marchi S., McCord T. B., McSween H. Y., Capaccioni F., Capria M. T., Carrozzo F. G., Ciarniello M., Longobardo A., Tosi F., Fonte S., Formisano M., Frigeri A., Giardino M., Magni G., Palomba E., Turrini D., Zambon F., Combe J.-P., Feldman W., Jaumann R., McFadden L. A., Pieters C. M., Prettyman T., Toplis M., Raymond C. A., and Russell C. T. 2015. Ammoniated phyllosilicates with a likely outer solar system origin on (1) Ceres. *Nature* 528:241–244.

De Sanctis M. C., Raponi A., Ammannito E., Ciarniello M., Toplis M. J., McSween H. Y., Castillo-Rogez J. C., Ehlmann B. L., Carrozzo F. G., Marchi S., Tosi F., Zambon F., Capaccioni F., Capria M. T., Fonte S., Formisano M., Frigeri A., Giardino M., Longobardo A., Magni G., Palomba E., McFadden L. A., Pieters C. M., Jaumann R., Schenk P., Mugnuolo R., Raymond C. A., and Russell C. T. 2016. Bright carbonate deposits as evidence of aqueous alteration on (1) Ceres. *Nature* 536:54–57.

De Sanctis M. C., Ammannito E., McSween H. Y., Raponi A., Marchi S., Capaccioni F., Capria M. T., Carrozzo F. G., Ciarniello M., Fonte S., Formisano M., Frigeri A., Giardino M., Longobardo A., Magni G., McFadden L. A., Palomba E., Pieters C. M., Tosi F., Zambon F., Raymond C. A., and Russell C. T. 2017. Localized aliphatic organic materials on the surface of Ceres. *Science* 355:719–722.

Erickson K., Erni R., Lee Z., Alem N., Gannett W., and Zettl A. 2010. Determination of the local chemical structure of graphene oxide and reduced graphene oxide. *Advanced Materials* 22:4467–4472.

Ferrari A. C. and Robertson J. 2001. Resonant Raman spectroscopy of disordered, amorphous, and diamondlike carbon. *Physical Review B* 64:1–13.

Glein C. R., Baross J. A., and Waiter J. H. 2015. The pH of Enceladus' ocean. *Geochimica et Cosmochimica Acta* 162:202–219.

Goesmann F., Rosenbauer H., Bredehöft J. H., Cabane M., Ehrenfreund P., Gautier T., Giri C., Krüger H., Le Roy L., MacDermott A. J., McKenna-Lawlor S., Meierhenrich U. J., Muñoz Caro G. M., Raulin F., Roll R., Steele A., Steininger H., Sternberg R., Szopa C., Thiemann W., and Ulamec S. 2015. Organic compounds on comet 67P/Churyumov-Gerasimenko revealed by COSAC mass spectrometry. *Science* 349:1–3.

Greenberg J. M., Shalabiea O. M., Mendoza-Gómez C. X., Schutte W., and Gerakines P. A. 1995. Origin of organic matter in the protoplanetary nebula and in comets. *Advances in Space Research* 16:9–16.

Greinke R. A. and Lewis I. C. 1984. Carbonization of naphthalene and dimethylnaphthalene. *Carbon* 22:305–314.

Hill H. G. M. and Nuth J. A. 2003. The catalytic potential of cosmic dust: Implications for prebiotic chemistry in the Solar nebula and other protoplanetary systems. *Astrobiology* 3:291–303.

Hsu H.-W., Postberg F., Sekine Y., Shibuya T., Kempf S., Horányi M., Juhász A., Altobelli N., Suzuki K., Masaki Y., Kuwatani T., Tachibana S., Sirono S.-I., Moragas-Klostermeyer G., and Srama R. 2015. Ongoing hydrothermal activities within Enceladus. *Nature* 519:207–210.

Kebukawa Y., Kilcoyne A. L. D., and Cody G. D. 2013. Exploring the potential formation of organic solids in chondrites and comets through polymerization of interstellar formaldehyde. *The Astrophysical Journal* 771:1–12.

Kobayashi T. 2014. Direct observation of large shock impedance jump upon shock-induced densification of powdered materials confirmed by in situ shock pressure and particle velocity measurements. *Chemical Physics Letters* 608:157–160.

Kobayashi T. 2016. Shock-wave-induced luminescence of phosphor powders. *Chemical Physics Letters* 643:43–46.

Llorca J. and Casanova I. 2000. Reaction between H_2, CO, and H_2S over Fe, Ni metal in the solar nebula: Experimental evidence for the formation of sulfur-bearing organic molecules and sulfides. *Meteoritics & Planetary Science* 35:841–848.

Marsh S. P. 1980. *LASI shock Hugoniot data*. Berkeley: University of California Press. 658 p.

McCulloch D. G., Prawer S., and Hoffman A. 1994. Structural investigation of Zenon-ion-beam-irradiated glassy carbon. *Physical Review B* 50:5905–5917.

McKay C. P., Anbar A. D., Porco C., and Tsou P. 2014. Follow the plume: The habitability of Enceladus. *Astrobiology* 14:352–355.

Melosh H. J. 1989. *Impact cratering: A geologic process*. New York: Oxford University Press.

Mimura K., Toyama S., and Sugitani K. 2005. Shock-induced dehydration of polycyclic aromatic hydrocarbons with or without serpentine: Implications for planetary accretion. *Earth & Planetary Science Letters* 232:143–156.

Ogawa N. O., Nagata T., Kitazato H., and Ohkouchi N. 2010. Ultra sensitive elemental analyzer/isotope ratio mass spectrometer for stable nitrogen and carbon isotopic analyses. In *Earth, life and isotopes*, edited by Ohkouchi N., Tayasu I., and Koba K. Kyoto: Kyoto University Press. pp. 339–353.

Postberg F., Schmidt J., Hillier J., Kempf S., and Srama R. 2011. A salt-water reservoir as the source of a compositionally stratified plume on Enceladus. *Nature* 474:620–622.

Postberg F., Khawaja N. A., Kempf S., Waite J. H., Glein C., Hsu H. W., and Srama R. 2017. Complex organic macromolecular compounds in ice grains from Enceladus (abstract #1401). 48th Lunar & Planetary Science Conference. CD-ROM.

Quirico E., Raynal P.-I., and Bourot-Denise M. 2003. Metamorphic grade of organic matter in six unequilibrated ordinary chondrites. *Meteoritics & Planetary Science* 38:795–811.

Quirico E., Rouzaud J.-N., Bonal L., and Montagnac G. 2005. Maturation grade of coals as revealed by Raman spectroscopy: Progress and problems. *Spectrochimica Acta Part A* 61:2368–2377.

Quirico E., Montagnac G., Rouzaud J.-N., Bonal L., Bourot-Denise M., Duber S., and Reynard B. 2009. Precursor and metamorphic condition effects on Raman spectra of poorly ordered carbonaceous matter in chondrites and coals. *Earth & Planetary Science Letters* 287:185–193.

Quirico E., Orthous-Daunay F.-R., Beck P., Bonal L., Brunetto R., Dartois E., Pino T., Montagnac G., Rouzaud J.-N., Engrand C., and Duprat J. 2014. Origin of insoluble organic matter in type 1 and 2 chondrites: New clues, new questions. *Geochimica et Cosmochimica Acta* 136:80–99.

Rapson W. S. and Robinson R. 1935. Experiments on the synthesis of substances related to sterols. Part II. A new general method for the synthesis of substituted cyclohexenes. *Journal of Chemical Society* 1285–1288.

Remusat L., Derenne S., and Robert F. 2005. New insight on aliphatic linkages in the macromolecular organic fraction of Orgueil and Murchison meteorites through ruthenium tetroxide oxidation. *Geochimica et Cosmochimica Acta* 69:4377–4386.

Ricardo A., Carrigan M. A., Olcott A. N., and Benner S. A. 2004. Borate minerals stabilize ribose. *Science* 303:196.

Saiki T., Imamura H., Arakawa M., Wada K., Takagi Y., Hayakawa M., Shirai K., Yano H., and Okamoto C. 2016. The Small Carry-on Impactor (SCI) and the Hayabusa2 impact experiment. *Space Science Reviews* 208:165–186.

Sandford S. A., Aléon J., Alexander C. M. O'D., Araki T., Bajt S., Baratta G. A., Borg J., Bradley J. P., Brownlee D. E., Brucato J. R., Burchell M. J., Busemann H., Butterworth A., Clemett S. J., Cody G., Colangeli L., Cooper G., D'Hendecourt L., Djouadi Z., Dworkin J. P., Ferrini G., Fleckenstein H., Flynn G. J., Franchi I. A., Fries M., Gilles M. K., Glavin D. P., Gounelle M., Grossemy F., Jacobsen C., Keller L. P., David Kilcoyne A. L., Leitner J., Matrajt G., Meibom A., Mennella V., Mostefaoui S., Nittler L. R., Palumbo M. E., Papanastassiou D. A., Robert F., Rotundi A., Snead C. J., Spencer M. K., Stadermann F. J., Steele A., Stephan T., Tsou P., Tyliszczak T., Westphal A. J., Wirick S., Wopenka B., Yabuta H., Zare R. N., and Zolensky M. E. 2006. Organic captured from comet 81P/Wild2 by the Stardust spacecraft. *Science* 314:1720–1724.

Sekine T. 1997. Shock wave chemical synthesis. *European Journal of Solid State and Inorganic Chemistry* 34:823–833.

Sekine Y., Sugita S., Shido T., Yamamoto T., Iwasawa Y., Kadono T., and Matsui T. 2005. The role of Fischer-Tropsch catalysis in the origin of methane-rich Titan. *Icarus* 178:154–164.

Sekine Y., Sugita S., Shido T., Yamamoto T., Iwasawa Y., Kadono T., and Matsui T. 2006. An experimental study on Fischer-Tropsch catalysis: Implications for impact phenomena and nebular chemistry. *Meteoritics & Planetary Science* 41:715–729.

Sekine Y., Takano Y., Yano H., Funase R., Takai K., Ishihara M., Shibuya T., Tachibana S., Kuramoto K., Yabuta H., Kimura J., and Furukawa Y. 2014. Exploration of Enceladus' water-rich plumes toward understanding of chemistry and biology of the interior ocean. *Transactions of the Japan Society for Aeronautical and Space Sciences, Aerospace Technology Japan* 12:7–11.

Sekine Y., Shibuya T., Postberg F., Hsu H.-W., Suzuki K., Masaki Y., Kuwatani T., Mori M., Hong P. K., Yoshizaki M., Tachibana S., and Sirono S.-I. 2015. High-temperature water-rock interactions and hydrothermal environments in the chondrite-like core of Enceladus. *Nature Communications* 6:1–8.

Sekine Y., Genda H., Kamata S., and Funatsu T. 2017. The Charon-forming giant impact as a source of Pluto's dark equatorial regions. *Nature Astronomy* 1:1–6.

Sephton M. A., Verchovsky A. B., Bland P. A., Gilmour I., Grady M. M., and Wright I. P. 2003. Investigating the variations in carbon and nitrogen isotopes in carbonaceous chondrites. *Geochimica et Cosmochimica Acta* 67:2093–2108.

Sephton M. A., Love G. D., Watson J. S., Verchovsky A. B., Wright I. P., Snape C. E., and Gilmour I. 2004. Hydropyrolysis of insoluble carbonaceous matter in the Murchison meteorite: New insights into its macromolecular structure. *Geochimica et Cosmochimica Acta* 68:1385–1393.

Sugita S., Kadono T., Ohno S., Hamano K., and Matsui T. 2003. Does laser ablation vapor simulate impact vapor? (abstract #1573). 34th Lunar & Planetary Science Conference. CD-ROM.

Tachibana S., Tachibana S., Abe M., Arakawa M., Fujimoto M., Iijima Y., Ishiguro M., Kitazato K., Kobayashi N., Namiki N., Okada T., Okazaki R., Sawada H., Sugita S., Takano Y., Tanaka S., Watanabe S., Yoshikawa M., Kuninaka H., and The Hayabusa2 Project Team. 2014. Hayabusa2: Scientific importance of samples returned from near-Earth C-type asteroid 1999 JU_3. *Geochemical Journal* 48:571–587.

Takano Y., Yano H., Sekine Y., Funase R., and Takai K. 2014. Planetary protection on international waters: An onboard protocol for capsule retrieval and biosafety control in sample return mission. *Advances in Space Research* 53:1135–1142.

Tayasu I., Hirasawa R., Ogawa N. O., Ohkouchi N., and Yamada K. 2011. New organic reference materials for carbon- and nitrogen-stable isotope ratio measurements provided by Center for Ecological Research, Kyoto University, and Institute of Biogeosciences, Japan Agency for Marine-Earth Science and Technology. *Limnology* 12:261–266.

Tsou P., Brownlee D. E., McKay C. P., Anbar A. D., Yano H., Altwegg K., Beegle L. W., Dissly R., Strange N. J., and Kanik I. 2012. LIFE: Life Investigation For Enceladus a sample return mission concept in search for evidence of life. *Astrobiology* 12:730–742.

Waite J. H., Lewis W. S., Magee B. A., Lunine J. I., McKinnon W. B., Glein C. R., Mousis O., Young D. T., Brockwell T., Westlake J., Nguyen M.-J., Teolis B. D., Niemann H. B., McNutt R. L. Jr., Perry M., and Ip W.-H. 2009. Liquid water on Enceladus from observations of ammonia and ^{40}Ar in the plume. *Nature* 460:487–490.

Waite J. H., Glein C. R., Perryman R. S., Teolis B. D., Magee B. A., Miller G., Grimes J., Perry M. E., Miller K. E., Bouquet A., Lunine J. I., Brockwell T., and Bolton S. J. 2017. Cassini finds molecular hydrogen in the Enceladus plume: Evidence for hydrothermal processes. *Science* 356:155–159.

Watanabe S., Tsuda Y., Yoshikawa M., Tanaka S., Saiki T., and Nakazawa S. 2017. Hayabusa2 mission overview. *Space Science Reviews* 208:3–16.

Yabuta H., Naraoka H., Sakanishi K., and Kawashima H. 2005. Solid-state ^{13}C NMR characterization of insoluble organic matter from Antarctic CM2 chondrites: Evaluation of the meteoritic alteration level. *Meteoritics & Planetary Science* 40:779–787.

Yabuta H., Alexander C. M. O'D., Fogel M. L., Kilcoyne A. L. D., and Cody G. D. 2010. A molecular and isotopic study of the macromolecular organic matter of the ungrouped C2 WIS 91600 and its relationship to Tagish Lake and PCA 91008. *Meteoritics & Planetary Science* 45:1446–1460.

Yang D., Velamakanni A., Bozoklu G., Park S., Stoller M., Piner R. D., Stankovich S., Jung I., Field D. A., Ventrice C. A. Jr., and Ruoff R. S. 2009. Chemical analysis of graphene oxide films after heat and chemical treatments by X-ray photoelectron and micro-Raman spectroscopy. *Carbon* 47:145–152.

Zolotov M. Y. 2012. Aqueous fluid composition in CI chondritic materials: Chemical equilibrium assessments in closed systems. *Icarus* 220:713–729.

SUPPORTING INFORMATION

Additional supporting information may be found in the online version of this article:

Table S1. Evaluation of effect of the pretreatment and laser irradiation on the Raman parameters.

Fig. S1. Evaluation of effect of the pretreatment for IR spectra of OSPBs.